



# Comparative proteomics analysis for identifying the lipid metabolism related pathways in patients with Klippel-Feil syndrome

Ziquan Li<sup>1,2</sup>, Cong Zhang<sup>3</sup>, Bintao Qiu<sup>4</sup>, Yuchen Niu<sup>4</sup>, Ling Leng<sup>4</sup>, Siyi Cai<sup>1,5</sup>, Ye Tian<sup>1</sup>, Terry Jianguo Zhang<sup>1,2,5</sup>, Guixing Qiu<sup>1,2,5</sup>, Nan Wu<sup>1,2,5</sup><sup>^</sup>, Zhihong Wu<sup>2,4,5</sup>, Yipeng Wang<sup>1,2,5</sup><sup>^</sup>

<sup>1</sup>Department of Orthopedic Surgery, Peking Union Medical College Hospital, Peking Union Medical College and Chinese Academy of Medical Sciences, Beijing, China; <sup>2</sup>Beijing Key Laboratory for Genetic Research of Skeletal Deformity, Beijing, China; <sup>3</sup>Department of Endocrinology, China-Japan Friendship Hospital, Beijing, China; <sup>4</sup>State Key Laboratory of Complex Severe and Rare Diseases, Peking Union Medical College Hospital, Peking Union Medical College and Chinese Academy of Medical Sciences, Beijing, China; <sup>5</sup>Key laboratory of big data for spinal deformities, Chinese Academy of Medical Sciences, Beijing, China

**Contributions:** (I) Conception and design: Z Li, N Wu, Z Wu; (II) Administrative support: TJ Zhang, Y Wang, G Qiu; (III) Provision of study materials or patients: C Zhang, S Cai, Y Tian; (IV) Collection and assembly of data: Y Niu, L Leng, B Qiu, Z Li; (V) Data analysis and interpretation: L Leng, B Qiu; (VI) Manuscript writing: All authors; (VII) Final approval of manuscript: All authors.

**Correspondence to:** Yipeng Wang MD, Department of Orthopedic Surgery, Beijing Key Laboratory for Genetic Research of Skeletal Deformity, Key Laboratory of Big Data For Spinal Deformities, Peking Union Medical College Hospital, Peking Union Medical College and Chinese Academy of Medical Sciences, No. 1 Shuaifuyuan, Beijing 100730, China. Email: ypwang@vip.126.com; Zhihong Wu, PhD, Beijing Key Laboratory for Genetic Research of Skeletal Deformity, State Key Laboratory of Complex Severe and Rare Diseases, Key Laboratory of Big Data for Spinal Deformities, Peking Union Medical College Hospital, Peking Union Medical College and Chinese Academy of Medical Sciences, No. 1 Shuaifuyuan, Beijing 100730, China. Email: wuzh3000@126.com.

**Background:** Klippel-Feil syndrome (KFS) represents the rare and complex deformity characterized by congenital defects in the formation or segmentation of the cervical vertebrae. There is a wide gap in understanding the detailed mechanisms of KFS because of its rarity, heterogeneity, small pedigrees, and the broad spectrum of anomalies.

**Methods:** We recruited eight patients of Chinese Han ethnicity with KFS, five patients with congenital scoliosis (CS) who presented with congenital fusion of the thoracic or lumbar spine and without known syndrome or cervical deformity, and seven healthy controls. Proteomic analysis by data-independent acquisition (DIA) was performed to identify the differential proteome among the three matched groups and the data were analyzed by bioinformatics tools including Gene Ontology (GO) categories and Ingenuity Pathway Analysis (IPA) database, to explore differentially abundant proteins (DAPs) and canonical pathways involved in the pathogenesis of KFS.

**Results:** A total of 49 DAPs were detected between KFS patients and the controls, and moreover, 192 DAPs were identified between patients with KFS and patients with CS. Fifteen DAPs that were common in both comparisons were considered as candidate biomarkers for KFS, including membrane primary amine oxidase, noelin, galectin-3-binding protein, cadherin-5, glyceraldehyde-3-phosphate dehydrogenase, peroxiredoxin-1, CD109 antigen, and eight immunoglobulins. Furthermore, the same significant canonical pathways of LXR/RXR activation and FXR/RXR activation were observed in both comparisons. Seven of DAPs were apolipoproteins related to these pathways that are involved in lipid metabolism.

**Conclusions:** This study provides the first proteomic profile for understanding the pathogenesis and identifying predictive biomarkers of KFS. We detected 15 DAPs that were common in both comparisons as candidate predictive biomarkers of KFS. The lipid metabolism-related canonical pathways of LXR/RXR and

<sup>^</sup> ORCID: Nan Wu, 0000-0002-9429-2889; Yipeng Wang, 0000-0001-9769-9839.

FXR/RXR activation together with seven differentially abundant apolipoproteins may play significant roles in the etiology of KFS and provide possible pathogenesis correlation between KFS and CS.

**Keywords:** Klippel-Feil syndrome (KFS); lipid metabolism; congenital scoliosis (CS); differentially abundant proteins (DAPs); LXR/RXR activation; FXR/RXR activation

Submitted Jul 07, 2020. Accepted for publication Nov 13, 2020.

doi: 10.21037/atm-20-5155

View this article at: <http://dx.doi.org/10.21037/atm-20-5155>

## Introduction

Klippel-Feil syndrome (KFS) is a relatively rare and complicated condition that is characterized as congenital fusion of two or more cervical vertebrae with or without additional spinal or extraspinal manifestations (1,2). It is estimated to occur one in every 40,000 to 42,000 births (3). However, the prevalence of KFS may be much higher because its diagnosis can be missed due to heterogeneity in phenotypic expression between patients (4-6). Patients with KFS show the clinical triad of short neck, low posterior hairline, and limited cervical range of motion (7). Congenital cervical fusion deformity often alters the kinematics of the cervical spine, leading to acceleration of degenerative manifestations, hypermobility and instability, neurologic symptoms, and the potential for neurological spinal injury after major or even minor trauma (8,9). As a consequence, KFS may result in serious physical and mental problems in patients. Studies have shown that, in KFS, the congenital fusion of the cervical spine is associated with failure of formation and segmentation embryologically (8). Mutated genes such as *GDF6*, *MEOX1*, *GDF3*, *MYO18B*, and *RIPPLY2* encode proteins involved in somite development via transcription regulation and signaling pathways (10-14). Although significant progress has been made in understanding the process of cervical vertebra fusion, there is a wide gap in understanding of the detailed mechanisms of KFS because of its rarity, heterogeneity, small pedigrees, and the broad spectrum of anomalies (15).

Thus, it is essential to explore early specific biomarkers and design measures to prevent potentially fatal outcomes in KFS patients. Data-independent acquisition (DIA) based quantitative proteomics analysis is a powerful mass spectrometric (MS) technique to perform both protein identification and quantification of complex protein samples (16,17). Furthermore, DIA method has been performed in biomarker studies to understand the pathogenesis and underlying mechanisms of congenital diseases (18-20).

Therefore, proteomics by DIA coupled with Q-Exactive mass spectrometry was used to compare the serum protein profiles of patients with KFS and healthy controls as well as patients with KFS and patients with congenital scoliosis (CS; patients with known syndromes and cervical deformity were excluded).

We present the following article in accordance with the MDAR checklist (available at <http://dx.doi.org/10.21037/atm-20-5155>).

## Methods

### *Patients and blood collection*

We consecutively recruited eight patients of Chinese Han ethnicity with KFS, who had fulfilled inclusion criteria of the congenital fusion of at least two cervical vertebrae, in the Peking Union Medical College Hospital from October 2018 to May 2019. Four were male and four were female, and the mean age at diagnosis was 21.0±13.4 years. Seven healthy control participants and five patients with CS were recruited with the sex and age matched. The patients with CS were presented with congenital fusion of the thoracic or lumbar spine and had no known syndrome and cervical deformity. The healthy controls had no congenital skeletal malformations which were confirmed by spine X-ray.

Blood samples were drawn from all the participants and centrifuged at 16,000 ×g (4 °C) for 10 min. The serum from each sample was transferred into new Eppendorf tubes and stored at -80 °C until used. Demographic information, clinical symptoms, detailed comorbidities, and radiological assessments of all the participants also were obtained (Table S1).

The study was conducted in accordance with the Declaration of Helsinki (as revised in 2013). The study was approved by ethics board of the Peking Union Medical College Hospital (No. JS-098) and informed consent was taken from all individual participants.

### *Sample preparation*

ProteoPrep Blue Albumin and an IgG Depletion kit (PROTBA, Sigma-Aldrich Company, Darmstadt, Germany) were used to deplete serum IgG and albumin. We used 10  $\mu$ L serums for the depletion, and 1 mL was eluted at the end of the procedure. The Bradford method was used to measure the protein concentration after depletion and vacuum concentration according to the manufacturer's instructions. Next, 40  $\mu$ g protein lysate was reduced with 25 mM DTT at 60 °C for 60 min and alkylated with 50 mM iodoacetamide in the dark for 30 min. After alkylation, FASP digestion was performed for each sample using an ultrafiltration filter (10 kDa cutoff, Sartorius, German). Trypsin was added in a 1:100 ratio (enzyme:protein) at 37 °C for 14–16 h, after which the samples were centrifuged at 20,000  $\times$ g (4 °C) for 10 min. The peptides were desalted using Ziptip C18 pipette tips (Merck KGaA, Darmstadt, Germany). After drying, the peptides were resuspended in 0.1% formic acid. Then, 20  $\mu$ g protein lysate was taken out of each sample and used to build the DIA Spectral Library. The Biognosys' iRT kit was added to the rest of the samples according to the manufacturer's instructions (required for DIA analysis using Biognosys' Spectronaut).

### *High pH reversed-phase fractionation*

High pH reversed-phase chromatography was applied to further fractionate the digests and 30  $\mu$ g of the digest was combined. The RIGOL L-3000 system (RIGOL, Beijing, China) was applied to the reverse-phase chromatography column to separate the peptides. The peptide mixtures were dissolved in 100  $\mu$ L mobile phase A (2% (v/v) acetonitrile, 98% (v/v) ddH<sub>2</sub>O; pH 10) and then centrifuged at 14,000  $\times$ g for 20 min. The supernatant was loaded into the column and eluted by continuously injecting mobile B (98% (v/v) acetonitrile, 2% (v/v) ddH<sub>2</sub>O; pH 10) at a flow rate of 700  $\mu$ L/min. A step gradient (1.5 min per step) of mobile phase B was used to elute and collect the fractions.

### *Mass spectrometric acquisition*

Each sample was analyzed using the analytical column (75  $\mu$ m  $\times$  250 mm; 2  $\mu$ m) in a nanoliquid chromatography system (EASY-nLC 1000 System, Thermo Scientific, Waltham, MA, USA) connected to a Q Exactive HF mass spectrometer (Thermo Scientific). A binary solvent system with 99.9% H<sub>2</sub>O, 0.1% formic acid (phase A) and 80% ACN,

19.9% H<sub>2</sub>O, 0.1% formic acid (phase B) was applied to elute the peptide mixtures. The following linear gradient was applied: 13–28% B in 93 min, 28–38% B in 11 min, 38–100% B in 4 min, and washed at 100% B for 8 min. The eluent was added directly into the Q-Exactive HF mass spectrometer via an EASY-Spray ion source. Source ionization parameters were as follows: spray voltage 2.2 kV, capillary temperature 320 °C, and declustering potential 100 V. One full-scan MS from 300 to 1,600 m/z, then 20 MS/MS scans were continuously acquired for data-dependent acquisition (DDA) LC-MS/MS analysis. The resolution was set to 60,000 for MS and 30,000 for MS/MS. For high-energy collisional dissociation, the isolation window was set to 2 m/z and the normalized collision energy was applied as 28%.

The DIA LC-MS/MS method relied on the MS1 scan from 300 to 1,100 m/z (AGC target of 36 or 80 ms injection time). DIA segments were collected at 30,000 resolutions (AGC target 2e5 and auto for injection time). The spectra were recorded in profile mode with collision energy 28%. The default charge state for the MS2 was set to 3. The raw mass spectrometric data, the spectral libraries, and the quantitative data tables have been deposited to the ProteomeXchange Consortium via the PRIDE partner repository.

### *Mass spectrometric data analysis and protein identification*

DIA analysis was performed on Spectronaut Pulsar, the mass spectrometer vendor-independent software from Biognosys. The false discovery rate was evaluated using the mProphet approach and was set to 1% at the peptide level. Protein inference was performed on the principle of parsimony using the ID picker algorithm implemented in Spectronaut. For the DIA analysis, the RAW files were converted to the Spectronaut file format and calibrated in the retention time dimension based on the global spectral library. The recalibrated files were used for the targeted data analysis without new recalibration of the retention time dimension.

Proteome Discoverer 2.1 analysis software with default settings (Trypsin/P, two missed cleavages) was applied for the DDA spectra. Search criteria included carbamidomethylation of cysteine as a fixed modification and oxidation of methionine and acetyl (protein N terminus) as variable modifications. The parent ion tolerance was 10 ppm and the fragment ion mass tolerance was 0.02 Da. The DDA files were searched against the human Swiss-

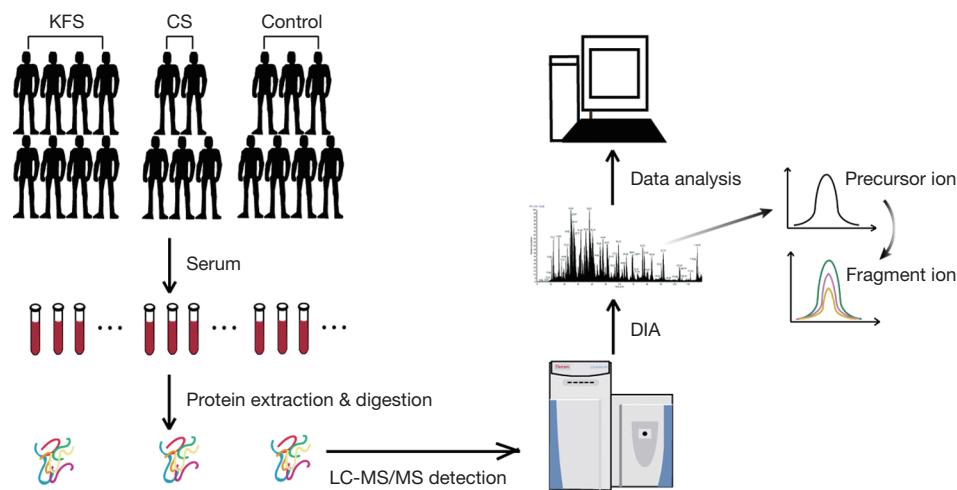


**Figure 1** Flowchart of the study design.

Prot fasta database (state 15.03.2018, 20,240 entries) and the Biognosys iRT peptides fasta database (uploaded to the public repository).

Procedures for sample preparation, high pH reversed-phase fractionation, LC-MS/MS and data analysis were shown in *Figure 1*.

### **Bioinformatics and statistical analyses**

The Perseus software was used to analyze the differences among the proteomic inventories in the two comparisons and the data were subjected to an analysis of variance test (two-sample *t*-tests). The cutoff values were set as 1.4-fold for increased and 0.71-fold for decreased abundance and the differential changes were considered significant at  $P \leq 0.05$ . The three main Gene Ontology (GO) categories, biological process, molecular function, and cellular component, were analyzed with OmicsBox (1.2.4) and pathway analysis was performed using the Ingenuity Pathway Analysis (IPA) database.

## **Results**

### **Identification and functional analysis of DAPs between patients with KFS and healthy controls**

We performed proteomic profiling of eight patients with KFS and seven healthy controls. A total of 493 proteins were identified and 49 of them were differentially abundant in the patients with KFS compared with the controls (ratio  $\geq 1.42$  or  $\leq 0.70$ ;  $P < 0.05$ ). Among the differentially abundant

proteins (DAPs), 27 were significantly decreased and 22 were significantly increased. Details of the 49 DAPs are presented in *Table S2* and their distribution is shown in the volcano plot in *Figure 2A*. A protein-protein interaction network was constructed using the DAPs that exhibited specific and extensive interactions and a score was calculated to assess the probability of protein-protein interactions that occurred by random chance (*Figure 2B*). The highest scoring network (score =18) included 10 target proteins related to cellular development, cellular growth and proliferation, and cellular movement. The DAPs were functionally annotated with GO terms under the three main categories: biological process, molecular function, and cellular component. Under biological process, the most enriched terms were related to regulation of cellular process, cellular response to stimulus, establishment of localization, and immune response. Under molecular function, the most enriched terms were protein binding, antigen binding, and ion binding. Under cellular components, the most enriched terms were extracellular space, plasma membrane, and cell periphery (*Figure 2C*).

### **Identification and functional analysis of DAPs between patients with KFS and patients with CS**

To further explore the correlated pathogenesis between KFS and CS and provide possible reasons for the deformity located at cervical segments, we performed proteomic profiling of patients with KFS and patients with CS. A total of 462 proteins were identified and 192 DAPs were differentially abundant in patients with KFS compared with patients with CS. Among them, 118 decreased and

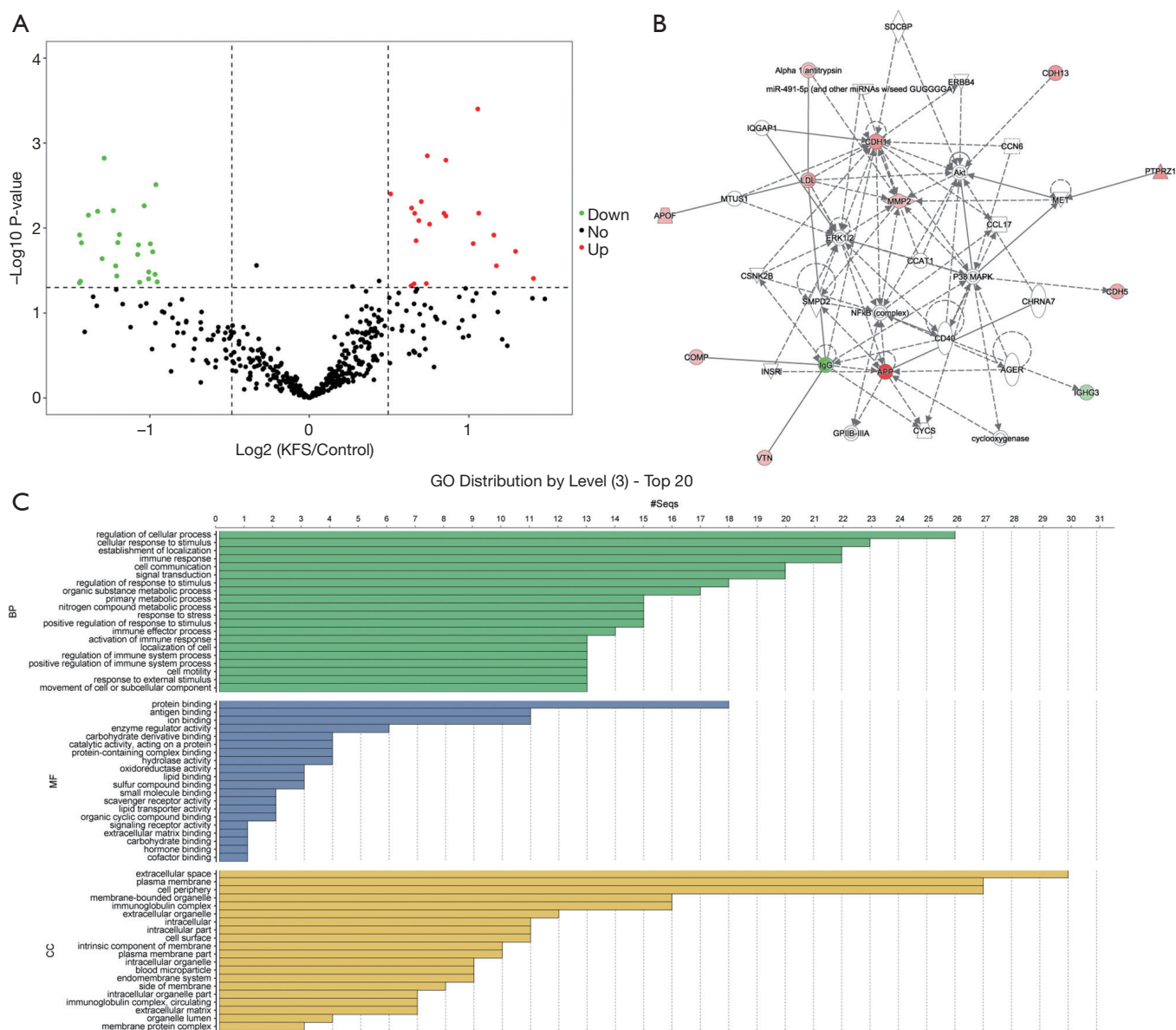


**Figure 2** Visualization and functional analysis of differentially abundant proteins (DAPs) in patients with Klippel-Feil syndrome (KFS) compared with healthy controls. (A) Volcano plot showing the 49 significant DAPs; 22 were increased and 27 were decreased. All the identified proteins (493) are plotted on the x-axis; the P values are plotted on the y-axis. Green, red, and gray dots indicate proteins with decreased, increased, and no change in abundance, respectively. (B) Protein-protein interaction network of the 49 DAPs. Solid lines indicate direct molecular interactions that have experimental confirmation; dashed lines indicate indirect interactions. Nodes in green and red indicate proteins with decreased and increased abundance, respectively. Uncolored nodes indicate potential target proteins that are functionally related to the DAPs. (C) Gene ontology (GO) functional annotation of the DAPs under the biological process (BP), molecular function (MF), and cellular component (CC) categories.

74 increased in abundance. Details of the 192 DAPs are presented in [Table S3](#). The DAPs were functionally annotated with GO terms. Under biological process, the most enriched term was regulation of cellular process, followed by organic substance metabolic process, primary metabolic process, cellular metabolic process, and nitrogen compound metabolic process. Under molecular function, the most enriched terms were protein binding and ion binding. Under cellular component, the most enriched terms were extracellular space and membrane-bounded organelle. The protein-protein interaction network with the highest score (score =37) included 25 target molecules associated with cancer, hematological disease, and inflammatory disease. The volcano plot, GO functional annotation, and protein-protein interaction network of these DAPs are shown in [Figure 3](#).

#### **Common DAPs in the two comparisons**

We selected 15 DAPs that were detected in both comparisons as candidate markers of KFS ([Table 1](#)). They included glyceraldehyde-3-phosphate dehydrogenase, CD109 antigen, cadherin-5, peroxiredoxin-1, galectin-3-binding protein, membrane primary amine oxidase, noelin, and eight immunoglobulins. A cluster analysis of the abundance levels of the 15 DAPs in patients with KFS, controls, and patients with CS showed that the abundance levels of eight immunoglobulins decreased significantly in patients with KFS or CS compared with the controls. Moreover, the decline in the abundance levels of immunoglobulins in patients with CS was more significantly than that in patients with KFS ([Figure 4](#)).

#### **Common canonical pathways in the two comparisons**

The distribution of the DAPs in the canonical pathways was calculated using the IPA software package. Pathways were considered to be significantly enriched for  $P < 0.05$ . The DAPs detected in the patients with KFS *vs.* controls comparison were involved in primary immunodeficiency signaling, hematopoiesis from pluripotent stem cells, communication between innate and adaptive immune cells, autoimmune thyroid disease signaling, phagosome formation, and LXR/RXR and FXR/RXR activation. The DAPs detected in the patients with KFS *vs.* patients with CS comparison were involved in crucial lipid metabolism-related pathways of LXR/RXR and FXR/RXR activation ([Figure 5](#)). The abundance levels of three key differentially

abundant lipoproteins, apolipoprotein C-III (APOC3), apolipoprotein A-IV (APOA4), and apolipoprotein F (APOF), were highly elevated in patients with KFS *vs.* controls, whereas the abundance levels of four other key lipoproteins, apolipoprotein A-II (APOA2), apolipoprotein E (APOE), apolipoprotein H (APOH: beta-2-glycoprotein I), and apolipoprotein D (APOD) were differentially abundant in the patients with KFS *vs.* patients with CS comparison; APOA2, APOE, and APOH were significantly reduced and APOD was highly elevated. All the DAPs involved in the LXR/RXR and FXR/RXR activation pathways, including the seven differentially abundant apolipoproteins, are shown in [Table 2](#).

## **Discussion**

KFS is a congenital cervical fusion malformation caused by segmentation defects in mesodermal somites (8,21,22). In this study, we employed a DIA method to explore 49 DAPs in patients with KFS compared with healthy controls. CS is a complex deformity of the spine caused by vertebral malformations, including defects of vertebral formation (hemivertebra or wedge vertebra) and defects of vertebral segmentation (vertebral bar or block vertebra) (23,24). Although CS and KFS both present with congenital vertebral malformation, whether there are potential pathogenic mechanisms between CS and KFS is largely unknown (25,26). Therefore, we performed a proteomic analysis of patients with KFS and patients with CS to detect predictive protein biomarkers of KFS and to explore the underlying mechanism between KFS and CS in somitogenesis. Overall, eight different immunoglobulins were detected among the 15 common DAPs in the two comparisons.

Immunoglobulins are glycoproteins that play roles in the immune system by specifically recognizing and binding to particular pathogens. Immunoglobulin kappa chain constant region (*IGKC*) was identified as a candidate gene that encodes a protein that may play a pivotal role in the autoimmune mechanism associated with the etiology of abdominal aortic aneurysm formation (27). In addition, *IGKC* was described as the B cell-related gene signature in human solid tumors, including breast, lung, and colorectal adenocarcinomas. *IGKC* is a novel diagnostic marker for risk stratification and the encoded protein may promote the humoral immune response in anticancer therapy (28). Moreover, immunogenetic studies suggested that *IGKC* and immunoglobulin heavy chain G (*IGHG*) contributed

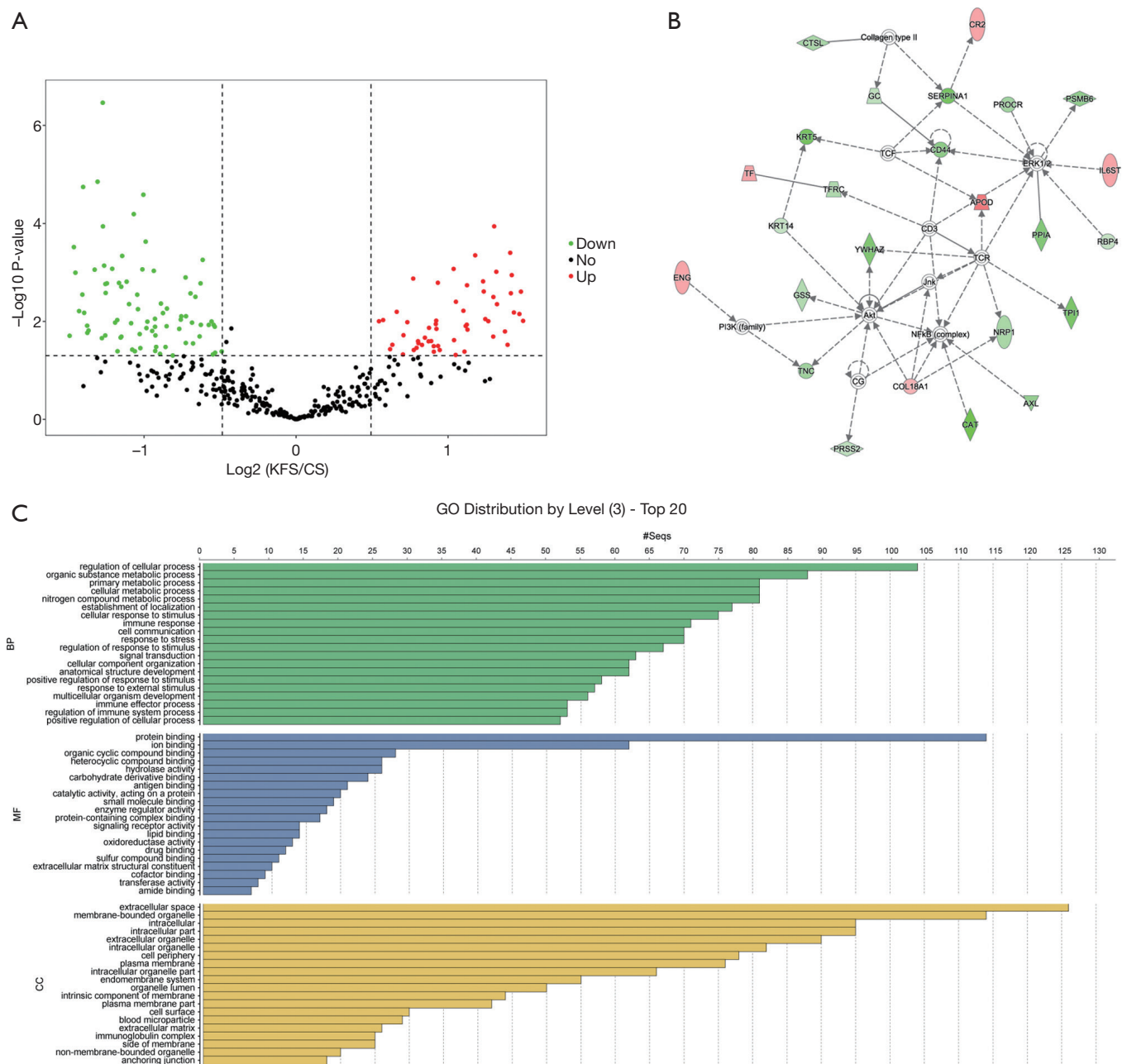


**Table 1** Differentially expressed proteins involved in both comparisons (KFS patients compared with control participants and CS patients)

Swiss-Prot accession no.	Swiss-Prot entry name	Protein Name	KFS patients/CS patients			KFS patients/control participants		
			P value	Fold change	Regulation	P value	Fold change	Regulation
P01834	IGKC_HUMAN	Immunoglobulin kappa constant	0.00039	3.73427	Up	0.01193	0.43808	Down
B9A064	IPLL5_HUMAN	Immunoglobulin lambda-like polypeptide 5	0.00012	2.46926	Up	0.02048	0.47431	Down
P0DOY2	IGLC2_HUMAN	Immunoglobulin lambda constant 2	0.00163	1.90980	Up	0.01578	0.47591	Down
A0A2Q2TTZ9	A0A2Q2TTZ9_HUMAN	Immunoglobulin kappa variable 1-33	0.00045	2.26433	Up	0.02794	0.43106	Down
P01857	IGHG1_HUMAN	Immunoglobulin heavy constant gamma 1	0.00015	3.06671	Up	0.03517	0.51085	Down
P01860	IGHG3_HUMAN	Immunoglobulin heavy constant gamma 3	0.00040	2.65677	Up	0.04317	0.51696	Down
P01599	KV117_HUMAN	Immunoglobulin kappa variable 1-17	0.03687	1.53585	Up	0.01533	0.50120	Down
P01718	LV327_HUMAN	Immunoglobulin lambda variable 3-27	0.04720	1.62870	Up	0.03967	0.49733	Down
Q06830	PRDX1_HUMAN	Peroxiredoxin-1	0.00115	0.24445	Down	0.01905	0.50629	Down
P04406	G3P_HUMAN	Glyceraldehyde-3-phosphate dehydrogenase	0.00073	0.41659	Down	0.00670	1.58071	Up
P33151	CADH5_HUMAN	Cadherin-5	0.01285	0.69025	Down	0.00159	1.81037	Up
Q6YHK3	CD109_HUMAN	CD109 antigen	0.02784	1.74779	Up	0.00721	1.81076	Up
Q08380	LG3BP_HUMAN	Galectin-3-binding protein	0.00705	2.77056	Up	0.00668	2.08792	Up
Q16853	AOC3_HUMAN	Membrane primary amine oxidase	0.00638	1.58299	Up	0.00141	1.66984	Up
Q99784	NOE1_HUMAN	Noelin	0.00085	2.05215	Up	0.00488	1.62694	Up

KFS, Klippel-Feil syndrome; CS, congenital scoliosis.

to the prognosis in breast cancer and to breast tumor-associated antigens in a racially restricted manner (29-31). However, our results are the first to account for the correlation between immunoglobulins and congenital spine deformities. The cluster analysis revealed a significant decline in the abundance levels of immunoglobulins, including IGHG1, IGHG3 and IGKC, in both patients with KFS and patients with CS compared with the healthy controls. These findings indicated that the low abundance of immunoglobulins may contribute to congenital vertebral malformation. We also found that immunoglobulins were

more abundant in serum samples of patients with KFS compared with those of patients with CS, which indicated that immunoglobulins may be valuable biomarkers for KFS. We deduced that dysfunction of the immune system may be the underlying pathogenic mechanism of somitogenesis defects in the cervical spine.

One of the 15 common DAPs, membrane primary amine oxidase, showed a more than 1.6-fold increase in patients with KFS compared with the controls. Membrane primary amine oxidase is highly abundant in endothelial cells, smooth muscle cells, and adipocytes (32) and is associated with

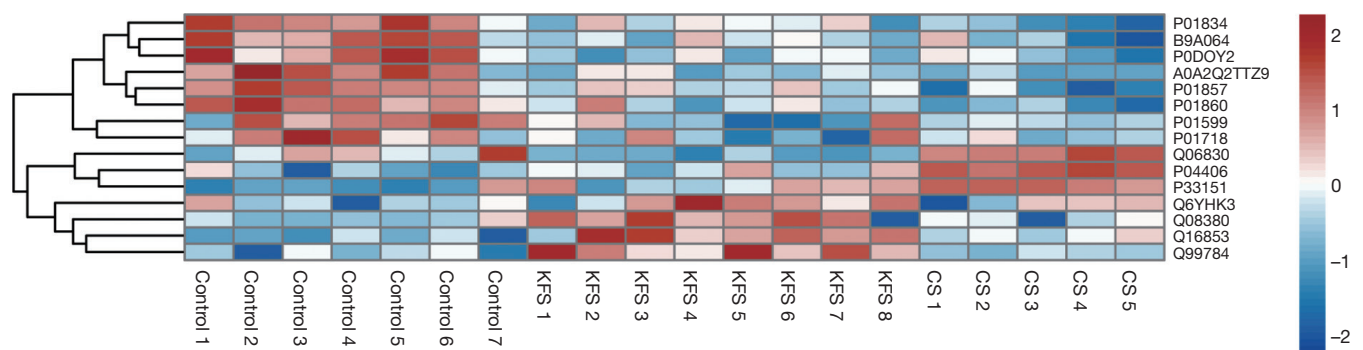


**Figure 4** Cluster analyses of differentially abundant proteins (DAPs) that were common in the patients with Klippel-Feil syndrome (KFS) *vs.* healthy controls and patients with KFS *vs.* patients with congenital scoliosis (CS) comparisons. The abundance levels of the 15 candidate DAPs in patients with KFS, patients with CS, and healthy controls are shown. Rows represent individual proteins; columns indicate individual participants. Blue indicates decreased protein abundance; red indicates increased protein abundance.

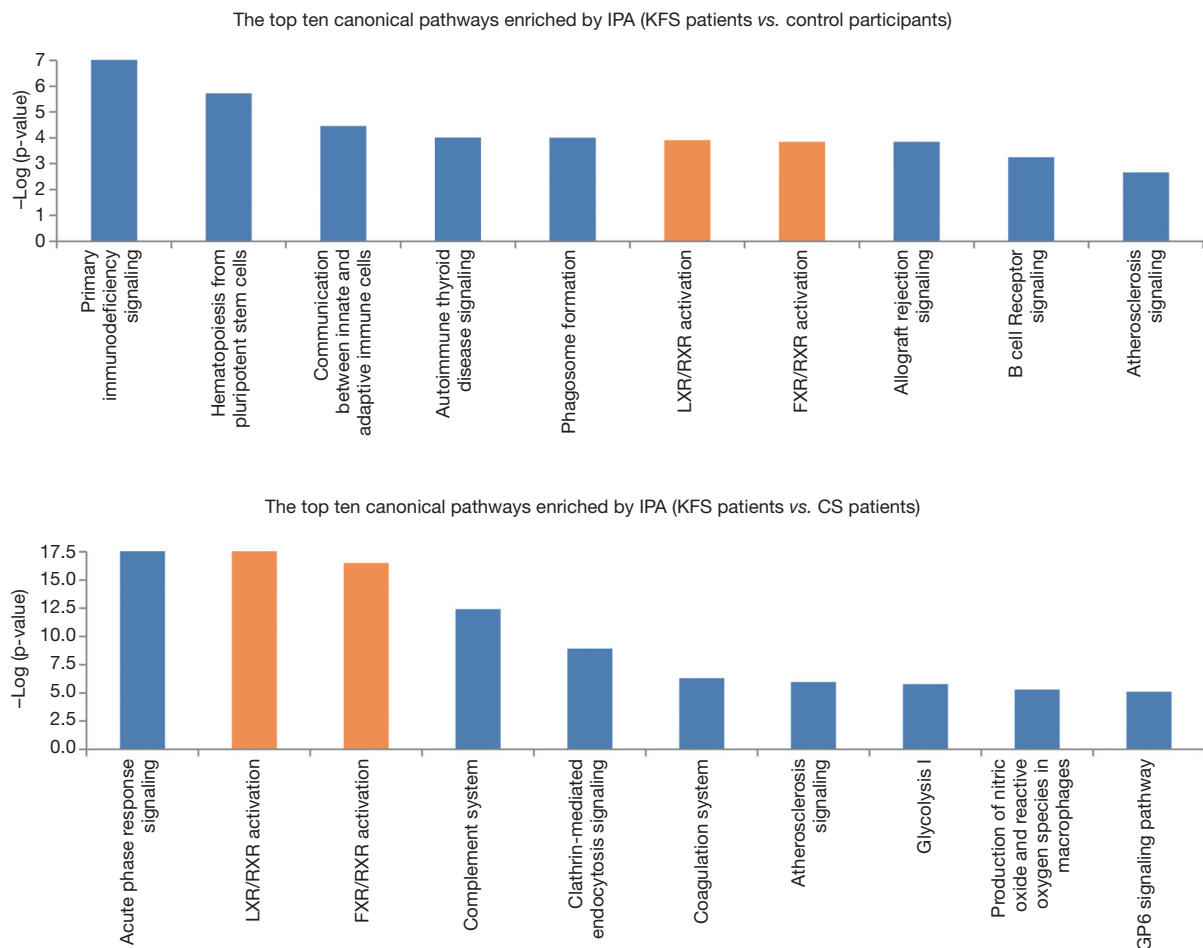


**Figure 5** Top ten canonical pathways that were common in the patients with Klippel-Feil syndrome (KFS) *vs.* healthy controls and patients with KFS *vs.* patients with congenital scoliosis (CS) comparisons. Differentially abundant proteins (DAPs) from the two comparisons were imported to the IPA software. The cellular signaling pathway histogram depicts the most relevant canonical pathways ranked by  $-\log(P)$  value). The LXR/RXR and FXR/RXR activation pathways were identified as common significant canonical pathways in both comparisons.

**Table 2** Differentially expressed proteins involved in LXR/RXR activation and FXR/RXR activation pathways

Swiss-Prot accession no.	Swiss-Prot entry name	Protein name	P value	Fold change
P05090	APOD_HUMAN	Apolipoprotein D	0.00576	3.589 (KFS/CS)
Q15166	PON3_HUMAN	Serum paraoxonase/lactonase 3	0.00097	2.493 (KFS/CS)
P02787	TRFE_HUMAN	Serotransferrin	0.04135	2.156 (KFS/CS)
P27169	PON1_HUMAN	Serum paraoxonase/arylesterase 1	0.00397	2.074 (KFS/CS)
P02765	FETUA_HUMAN	Alpha-2-HS-glycoprotein	0.00965	1.895 (KFS/CS)
P43652	AFAM_HUMAN	Afamin	0.02521	1.853 (KFS/CS)
Q9NPH3	IL1AP_HUMAN	Interleukin-1 receptor accessory protein	0.00938	1.488 (KFS/CS)
P02753	RET4_HUMAN	Retinol-binding protein 4	0.04721	0.684 (KFS/CS)
P02649	APOE_HUMAN	Apolipoprotein E	0.01181	0.671 (KFS/CS)
P02774	VTDB_HUMAN	Vitamin D-binding protein	0.00167	0.647 (KFS/CS)
P02652	APOA2_HUMAN	Apolipoprotein A-II	0.02753	0.605 (KFS/CS)
Q9UHG3	PCYOX_HUMAN	Prenylcysteine oxidase 1	0.00885	0.525 (KFS/CS)
P02671	FIBA_HUMAN	Fibrinogen alpha chain	0.00167	0.422 (KFS/CS)
P02749	APOH_HUMAN	Beta-2-glycoprotein 1	3.44E-07	0.414 (KFS/CS)
Q14624	ITIH4_HUMAN	Inter-alpha-trypsin inhibitor heavy chain H4	0.02197	0.412 (KFS/CS)
P08571	CD14_HUMAN	Monocyte differentiation antigen CD14	0.00220	0.321 (KFS/CS)
P01009	A1AT_HUMAN	Alpha-1-antitrypsin	0.00080	0.265 (KFS/CS)
P0DJ18	SAA1_HUMAN	Serum amyloid A-1 protein	0.00575	0.168 (KFS/CS)
P0DJ19	SAA2_HUMAN	Serum amyloid A-2 protein	0.01124	0.168 (KFS/CS)
P06727	APOA4_HUMAN	Apolipoprotein A-IV	0.01882	2.450 (KFS/Control)
P02656	APOC3_HUMAN	Apolipoprotein C-III	0.00670	1.795 (KFS/Control)
Q13790	APOF_HUMAN	Apolipoprotein F	0.04506	1.663 (KFS/Control)
P04004	VTNC_HUMAN	Vitronectin	0.04533	1.576 (KFS/Control)

KFS, Klippel-Feil syndrome; CS, congenital scoliosis.

several amino acid metabolism pathways by catalyzing the oxidative deamination of primary amines to aldehydes (33). Amino acid deficiency in the amniotic fluid was related to the pathogenesis of skeletal dysplasia in pregnant women with skeletal dysplasia fetuses (34). Further, protein tyrosine phosphatases were shown to play important roles in gastrulation and somitogenesis during early embryonic development, osteogenesis, and angiogenesis (35). Therefore, we propose that membrane primary amine oxidase could be a candidate biomarker related to amino acid metabolism in the pathogenesis of KFS. The other common DAPs, galectin-3-binding protein, glyceraldehyde-3-phosphate dehydrogenase, peroxiredoxin-1, CD109 antigen, cadherin-5, and noelin, have not previously

been reported to be related to KFS. They require further validation to establish their possible use as biomarkers for the etiological elucidation in KFS.

The IPA illustrated that the LXR/RXR and FXR/RXR activation pathways were common significant canonical pathways in the patients with KFS *vs.* controls and patients with KFS *vs.* patients with CS comparisons. All seven of the differentially abundant apolipoproteins (APOC3, APOA4, APOF, APOA2, APOE, APOH, and APOD) were involved these pathways. Retinoid X receptors (RXRs) are nuclear receptors that regulate a variety of physiological processes, including lipid metabolism, osteoclastogenesis, inflammatory response, and cell differentiation (36-38). Liver X receptors (LXRs) are ligand-activated transcription

factors that form a functional heterodimer with RXR through the LXR reaction element (39,40). LXR/RXR is considered to be involved in lipid metabolism and bile acid metabolism (41,42) and the formation of LXR/RXR heterodimers was shown to inhibit the transcriptional program of osteoclast differentiation (37). Farnesoid X receptors (FXRs) are members of the nuclear receptor family, which is involved in many metabolic pathways (43). FXR/RXR and LXR/RXR activation are involved in regulating osteogenic differentiation of adipose stem cells (44). These biological pathways detected in patients with KFS are consistent with the results of a previous comparative proteomics study by iTRAQ that explored the differential serum protein abundance levels of nine patients with CS who had *TBX6* haploinsufficiency and nine healthy controls (45). Several studies have shown that lipid metabolism is related to osteogenesis and musculoskeletal disorders. Nogami *et al.* reported that increased numbers of lipid droplets were detected in biopsied muscle fibers of two patients with congenital skeletal deformities such as scoliosis (46). van Gastel *et al.* revealed a role for forkhead box O transcription factors during lipid starvation and defined lipid scarcity as an important determinant of chondrogenic commitment (47). Rendina-Ruedy *et al.* suggested that lipids in the bone marrow are essential for proper bone remodeling (48). Vasiljevski *et al.* summarized neurofibromatosis type 1 and autoimmune myopathies (polymyositis, dermatomyositis, and inclusion body myositis) are involved in dysfunction of lipid metabolism (49). As such, our results and other evidence strongly point to disrupted lipid metabolism in KFS.

Apolipoprotein is plasma lipoprotein that is synthesized mainly in the liver (and partially in the small intestine) and transports lipids and stabilizes lipoproteins (50). APOE and APOA1 were shown to be highly abundant in the embryonic yolk syncytial layer and distributed in the form of cell clusters along the spinal cord, an extraembryonic structure implicated in embryonic and larval nutrition (51). It has been demonstrated that *APOE* was up-regulated by bone morphogenetic protein-2 in the murine mesenchymal progenitor cell and *APOE*<sup>-/-</sup> mice had significantly reduced levels of the osteoblastic (*RUNX2* and *Osterix*) and lipoblastic (*PPAR $\gamma$*  and *CEBP $\alpha$* ) indicators (52-54). These findings suggested that *APOE* played significant roles in embryonic differentiation as well as osteoblastic and lipoblastic differentiation and activity. The pathogenesis of congenital cervical fusion malformations have been

attributed to the paraxial mesoderm, somites, or central axis at the embryonic stage, possibly because of disruptions in differentiation and segmentation (55). Therefore, differentially abundant apolipoproteins and lipid metabolism-related molecules may play important roles in the development of paraxial mesoderm, somites, and the central axis, and may be involved in the pathogenesis of KFS and related vertebral segmentation defects.

The differentially abundant apolipoproteins and LXR/RXR and FXR/RXR activation pathways related to lipid metabolism led us to strongly speculate that lipid metabolism was involved in the underlying pathogenesis of KFS. Because somitogenesis generates vertebral structures in a rostral-to-caudal direction, we predict that the differentially abundant apolipoproteins detected in patients with KFS and patients with CS (e.g. *APOA2*, *APOD*, *APOE*, and *APOH*) could be significant biomarkers to investigate the possible mechanism associated with the vertebral segmental abnormalities located at cervical segments.

## Conclusions

We detected 15 DAPs that were common in both comparisons as candidate predictive biomarkers of KFS. The lipid metabolism-related canonical pathways of LXR/RXR and FXR/RXR activation together with seven differentially abundant apolipoproteins may play significant roles in the etiology of KFS and provide possible pathogenesis correlation between KFS and CS. The underlying interactions among the 15 DAPs and the progression of KFS require further investigation.

## Acknowledgments

The authors would like to thank all the patients and their family members for their help and informed consent.

**Funding:** This work was supported by the National Natural Science Foundation of China (No. 81871746 to YW, No. 81772299 and 81930068 to ZW, No. 81822030 to NW, No. 81672123 and 81972037 to JZ) and China Postdoctoral Science Foundation (No. 2020TQ0052 to ZL).

## Footnote

**Reporting Checklist:** The authors have completed the MDAR checklist. Available at <http://dx.doi.org/10.21037/atm-20-5155>

*Data Sharing Statement:* Available at <http://dx.doi.org/10.21037/atm-20-5155>

*Conflicts of Interest:* All authors have completed the ICMJE uniform disclosure form (available at <http://dx.doi.org/10.21037/atm-20-5155>). The authors have no conflicts of interest to declare.

*Ethical Statement:* The authors are accountable for all aspects of the work in ensuring that questions related to the accuracy or integrity of any part of the work are appropriately investigated and resolved. The study was conducted in accordance with the Declaration of Helsinki (as revised in 2013). The study was approved by ethics board of the Peking Union Medical College Hospital (NO. JS-098) and informed consent was taken from all individual participants.

*Open Access Statement:* This is an Open Access article distributed in accordance with the Creative Commons Attribution-NonCommercial-NoDerivs 4.0 International License (CC BY-NC-ND 4.0), which permits the non-commercial replication and distribution of the article with the strict proviso that no changes or edits are made and the original work is properly cited (including links to both the formal publication through the relevant DOI and the license). See: <https://creativecommons.org/licenses/by-nc-nd/4.0/>.

## References

- Samartzis D, Kalluri P, Herman J, et al. Cervical scoliosis in the Klippel-Feil patient. *Spine* 2011;36:E1501-8.
- Mesfin A, Bakhsh WR, Chuntarapas T, et al. Cervical Scoliosis: Clinical and Radiographic Outcomes. *Global Spine J* 2016;6:7-13.
- Juberg RC, Gershanik JJ. Cervical vertebral fusion (Klippel-Feil) syndrome with consanguineous parents. *J Med Genet* 1976;13:246-9.
- Xue X, Shen J, Zhang J, et al. Klippel-Feil syndrome in congenital scoliosis. *Spine* 2014;39:E1353-8.
- Gruber J, Saleh A, Bakhsh W, et al. The Prevalence of Klippel-Feil Syndrome: A Computed Tomography-Based Analysis of 2,917 Patients. *Spine Deform* 2018;6:448-53.
- Nouri A, Tetreault L, Zamorano JJ, et al. Prevalence of Klippel-Feil Syndrome in a Surgical Series of Patients with Cervical Spondylotic Myelopathy: Analysis of the Prospective, Multicenter AOSpine North America Study. *Global Spine J* 2015;5:294-9.
- Samartzis D, Kalluri P, Herman J, et al. "Clinical triad" findings in pediatric Klippel-Feil patients. *Scoliosis Spinal Disord* 2016;11:15.
- Tracy MR, Dormans JP, Kusumi K. Klippel-Feil syndrome: clinical features and current understanding of etiology. *Clin Orthop Relat Res* 2004;424:183-90.
- Nouri A, Patel K, Evans H, et al. Demographics, presentation and symptoms of patients with Klippel-Feil syndrome: analysis of a global patient-reported registry. *Eur Spine J* 2019;28:2257-65.
- Mohamed JY, Faqeih E, Alsiddiky A, et al. Mutations in MEOX1, encoding mesenchyme homeobox 1, cause Klippel-Feil anomaly. *Am J Hum Genet* 2013;92:157-61.
- Ye M, Berry-Wynne KM, Asai-Coakwell M, et al. Mutation of the bone morphogenetic protein GDF3 causes ocular and skeletal anomalies. *Hum Mol Genet* 2010;19:287-98.
- Alazami AM, Kentab AY, Faqeih E, et al. A novel syndrome of Klippel-Feil anomaly, myopathy, and characteristic facies is linked to a null mutation in MYO18B. *J Med Genet* 2015;52:400-4.
- Karaca E, Yuregir OO, Bozdogan ST, et al. Rare variants in the notch signaling pathway describe a novel type of autosomal recessive Klippel-Feil syndrome. *Am J Med Genet A* 2015;167A:2795-9.
- Tassabehji M, Fang ZM, Hilton EN, et al. Mutations in GDF6 are associated with vertebral segmentation defects in Klippel-Feil syndrome. *Hum Mutat* 2008;29:1017-27.
- Chacón-Camacho O, Camarillo-Blancarte L, Pelaez-González H, et al. Klippel-Feil syndrome associated with situs inversus: description of a new case and exclusion of GDF1, GDF3 and GDF6 as causal genes. *Eur J Med Genet* 2012;55:414-7.
- Nigjeh EN, Chen R, Brand RE, et al. Quantitative Proteomics Based on Optimized Data-Independent Acquisition in Plasma Analysis. *J Proteome Res* 2017;16:665-76.
- Reubsæet L, Sweredoski MJ, Moradian A. Data-Independent Acquisition for the Orbitrap Q Exactive HF: A Tutorial. *J Proteome Res* 2019;18:803-13.
- Parker SJ, Stotland A, MacFarlane E, et al. Proteomics reveals Rictor as a noncanonical TGF- $\beta$  signaling target during aneurysm progression in Marfan mice. *Am J Physiol Heart Circ Physiol* 2018;315:H1112-26.
- Kobayashi D, Tokuda T, Sato K, et al. Identification of a Specific Translational Machinery via TCTP-EF1A2 Interaction Regulating NF1-associated Tumor Growth by Affinity Purification and Data-independent Mass

- Spectrometry Acquisition (AP-DIA). *Mol Cell Proteomics* 2019;18:245-62.
20. Folkesson E, Turkiewicz A, Rydén M, et al. Proteomic characterization of the normal human medial meniscus body using data-independent acquisition mass spectrometry. *J Orthop Res* 2020;38:1735-45.
  21. Schieffer KM, Varga E, Miller KE, et al. Expanding the clinical history associated with syndromic Klippel-Feil: A unique case of comorbidity with medulloblastoma. *Eur J Med Genet* 2019;62:103701.
  22. Dauer MVP, Currie PD, Berger J. Skeletal malformations of Meox1-deficient zebrafish resemble human Klippel-Feil syndrome. *J Anat* 2018;233:687-95.
  23. Liu J, Wu N, Yang N, et al. TBX6-associated congenital scoliosis (TACS) as a clinically distinguishable subtype of congenital scoliosis: further evidence supporting the compound inheritance and TBX6 gene dosage model. *Genet Med* 2019;21:1548-58.
  24. Wu N, Ming X, Xiao J, et al. TBX6 null variants and a common hypomorphic allele in congenital scoliosis. *N Engl J Med* 2015;372:341-50.
  25. Cho W, Shepard N, Arlet V. The etiology of congenital scoliosis: genetic vs. environmental—a report of three monozygotic twin cases. *Eur Spine J* 2018;27:533-7.
  26. Klimo P, Rao G, Brockmeyer D. Congenital anomalies of the cervical spine. *Neurosurg Clin N Am* 2007;18:463-78.
  27. Kim DI, Eo HS, Joh JH. Differential expression of immunoglobulin kappa chain constant region in human abdominal aortic aneurysm. *J Surg Res* 2005;127:118-22.
  28. Schmidt M, Hellwig B, Hammad S, et al. A comprehensive analysis of human gene expression profiles identifies stromal immunoglobulin  $\kappa$  C as a compatible prognostic marker in human solid tumors. *Clin Cancer Res* 2012;18:2695-703.
  29. Pandey JP, Namboodiri AM, Armeson KE, et al. IGHG, IGKC, and FCGR genes and endogenous antibody responses to GARP in patients with breast cancer and matched controls. *Hum Immunol* 2018;79:632-7.
  30. Pandey JP, Kistner-Griffin E, Iwasaki M, et al. Genetic markers of immunoglobulin G and susceptibility to breast cancer. *Hum Immunol* 2012;73:1155-8.
  31. Oxelius VA, Pandey JP. Human immunoglobulin constant heavy G chain (IGHG) (Fc $\gamma$ ) (GM) genes, defining innate variants of IgG molecules and B cells, have impact on disease and therapy. *Clin Immunol* 2013;149:475-86.
  32. Elovaara H, Kidron H, Parkash V, et al. Identification of two imidazole binding sites and key residues for substrate specificity in human primary amine oxidase AOC3. *Biochemistry* 2011;50:5507-20.
  33. Carpéné C, Les F, Hasnaoui M, et al. Anatomical distribution of primary amine oxidase activity in four adipose depots and plasma of severely obese women with or without a dysmetabolic profile. *J Physiol Biochem* 2016;73:475-86.
  34. Kale E, Kale A. Amniotic fluid amino acid concentrations in fetal skeletal dysplasia. *Clin Exp Obstet Gynecol* 2014;41:280-2.
  35. Hale AJ, Ter Steege E, den Hertog J. Recent advances in understanding the role of protein-tyrosine phosphatases in development and disease. *Dev Biol* 2017;428:283-92.
  36. Lefebvre P, Benomar Y, Staels B. Retinoid X receptors: common heterodimerization partners with distinct functions. *Trends Endocrinol Metab* 2010;21:676-83.
  37. Menéndez-Gutiérrez MP, Röszer T, Fuentes L, et al. Retinoid X receptors orchestrate osteoclast differentiation and postnatal bone remodeling. *J Clin Invest* 2015;125:809-23.
  38. Röszer T, Menéndez-Gutiérrez MP, Cedenilla M, et al. Retinoid X receptors in macrophage biology. *Trends Endocrinol Metab* 2013;24:460-8.
  39. He Q, Wang F, Fan Y, et al. Differential effects of and mechanisms underlying the protection of cardiomyocytes by liver-X-receptor subtypes against high glucose stress-induced injury. *Biochem Biophys Res Commun* 2018;503:1372-7.
  40. Son YL, Lee YC. Molecular determinants of the interactions between SRC-1 and LXR/RXR heterodimers. *FEBS Lett* 2010;584:3862-6.
  41. Shen Q, Bai Y, Chang KC, et al. Liver X receptor-retinoid X receptor (LXR-RXR) heterodimer cistrome reveals coordination of LXR and AP1 signaling in keratinocytes. *J Biol Chem* 2011;286:14554-63.
  42. Wang B, Tontonoz P. Liver X receptors in lipid signalling and membrane homeostasis. *Nat Rev Endocrinol* 2018;14:452-63.
  43. Yang C, Zhou C, Li J, et al. Quantitative proteomic study of the plasma reveals acute phase response and LXR/RXR and FXR/RXR activation in the chronic unpredictable mild stress mouse model of depression. *Mol Med Rep* 2018;17:93-102.
  44. Zhao X, Liang M, Li X, et al. Identification of key genes and pathways associated with osteogenic differentiation of adipose stem cells. *J Cell Physiol* 2018;233:9777-85.
  45. Zhu Q, Wu N, Liu G, et al. Comparative analysis of serum proteome in congenital scoliosis patients with TBX6 haploinsufficiency - a first report pointing to lipid

- metabolism. *J Cell Mol Med* 2018;22:533-45.
46. Nogami H, Ogasawara N, Kasai T, et al. Lipid storage myopathy associated with scoliosis and multiple joint contractures. *Acta neuropathol* 1983;61:305-10.
  47. van Gastel N, Stegen S, Eelen G, et al. Lipid availability determines fate of skeletal progenitor cells via SOX9. *Nature* 2020;579:111-7.
  48. Rendina-Ruedy E, Rosen CJ. Lipids in the Bone Marrow: An Evolving Perspective. *Cell Metab* 2020;31:219-31.
  49. Vasiljevski ER, Summers MA, Little DG, et al. Lipid storage myopathies: Current treatments and future directions. *Prog Lipid Res* 2018;72:1-17.
  50. Mahley RW, Innerarity TL, Rall SC, et al. Plasma lipoproteins: apolipoprotein structure and function. *J Lipid Res* 1984;25:1277-94.
  51. Babin PJ, Thisse C, Durliat M, et al. Both apolipoprotein E and A-I genes are present in a nonmammalian vertebrate and are highly expressed during embryonic development. *Proc Natl Acad Sci U S A* 1997;94:8622-7.
  52. Niemeier A, Schinke T, Heeren J, et al. The role of apolipoprotein E in bone metabolism. *Bone* 2012;50:518-24.
  53. Zhang L, Li P, Tang Z, et al. Effects of GLP-1 receptor analogue liraglutide and DPP-4 inhibitor vildagliptin on the bone metabolism in ApoE mice. *Ann Transl Med* 2019;7:369.
  54. Papachristou NI, Blair HC, Kalyvoti ES, et al. Western-type diet differentially modulates osteoblast, osteoclast, and lipoblast differentiation and activation in a background of APOE deficiency. *Lab Invest* 2018;98:1516-26.
  55. Hubaud A, Pourquié O. Signalling dynamics in vertebrate segmentation. *Nat Rev Mol Cell Biol* 2014;15:709-21.

**Cite this article as:** Li Z, Zhang C, Qiu B, Niu Y, Leng L, Cai S, Tian Y, Zhang TJ, Qiu G, Wu N, Wu Z, Wang Y. Comparative proteomics analysis for identifying the lipid metabolism related pathways in patients with Klippel-Feil syndrome. *Ann Transl Med* 2021;9(3):255. doi: 10.21037/atm-20-5155

**Table S1** Demographic and clinical characteristics of participants

No.	Age at diagnosis	Sex	Group	Comorbidities	Fusion levels	Classification*
1	11	M	KFS	Torticollis	C2-3	I
2	35	F	KFS	Basilar invagination, Torticollis	C1-6	III
3	24	M	KFS	None	C2-4, C5-T1	II
4	13	F	KFS	Hypogonadism	C2-5	III
5	49	M	KFS	Cervical spondylosis	C4-5	I
6	8	M	KFS	None	C6-7	I
7	12	F	KFS	Syringomyelia, Ventricular hypertrophy	C6-7	I
8	16	F	KFS	None	C2-6	III
9	21	M	CS	Kyphosis	L1-2	II
10	14	M	CS	None	T4-5	III
11	47	F	CS	Diastematomyelia, Tethered cord, Kyphosis	T12-L1	III
12	11	M	CS	None	T5-8	III
13	3	F	CS	None	T11-12	II
14	20	M	Control	Right ankle fracture	None	None
15	21	F	Control	Lumbar disc herniation	None	None
16	25	F	Control	None	None	None
17	30	M	Control	Synovitis	None	None
18	26	M	Control	Hyperuricemia	None	None
19	10	M	Control	None	None	None
20	13	F	Control	Obstructive sleep apnea syndrome, Obesity	None	None

\*, KFS patients were evaluated based on following classification criteria: Type I, a single congenitally fused cervical segment; Type II, multiple noncontiguous congenitally fused cervical segments; Type III, multiple contiguous congenitally fused cervical segments. CS patients were evaluated based on following classification criteria. Type I, failure of segmentation; Type II, defects of formation; Type III, mixed form with both segmentation defect and failure of formation. KFS, Klippel-Feil syndrome; CS, congenital scoliosis.

**Table S2** Identification of 49 differentially expressed proteins in serum between KFS patients and control participants

Protein Accessions	Protein Descriptions	t-test P value	Ratio (KFS/Control)
P01861	Immunoglobulin heavy constant gamma 4	0.005	0.134
A0A087WSY4	Immunoglobulin heavy variable 4-30-2	0.025	0.295
A0A0G2JRK6	Uncharacterized protein	0.029	0.320
A0A0B4J1V2	Immunoglobulin heavy variable 2-26	0.044	0.368
P15814	Immunoglobulin lambda-like polypeptide 1	0.012	0.369
A0A087WSY6	Immunoglobulin kappa variable 3D-15	0.042	0.370
P01877	Immunoglobulin heavy constant alpha 2	0.015	0.371
A0A0C4DH67	Immunoglobulin kappa variable 1-8	0.007	0.383
P42785	Lysosomal Pro-X carboxypeptidase	0.006	0.399
A0A075B7B8	Immunoglobulin heavy variable 3/OR16-12	0.023	0.406
A0A0C4DH72	Immunoglobulin kappa variable 1-6	0.002	0.410
A0A075B6H7	Immunoglobulin kappa variable 3-7	0.006	0.427
A0A2Q2TTZ9	Immunoglobulin kappa variable 1-33	0.028	0.431
P01619	Immunoglobulin kappa variable 3-20	0.037	0.433
P01876	Immunoglobulin heavy constant alpha 1	0.015	0.435
P01834	Immunoglobulin kappa constant	0.012	0.438
B9A064	Immunoglobulin lambda-like polypeptide 5	0.020	0.474
P0DOY2;P0DOY3	Immunoglobulin lambda constant	0.016	0.476
A0A075B6K4	Immunoglobulin lambda variable 3-10	0.043	0.478
P01714	Immunoglobulin lambda variable 3-19	0.005	0.488
P01718	Immunoglobulin lambda variable 3-27	0.040	0.497
P01624	Immunoglobulin kappa variable 3-15	0.033	0.498
P01599	Immunoglobulin kappa variable 1-17	0.015	0.501
Q06830	Peroxiredoxin-1	0.019	0.506
P01857	Immunoglobulin heavy constant gamma 1	0.035	0.511
A0A0C4DH25	Immunoglobulin kappa variable 3D-20	0.003	0.513
P01860	Immunoglobulin heavy constant gamma 3	0.043	0.517
P05543	Thyroxine-binding globulin	0.004	1.424
Q86U17	Serpin A11	0.048	1.557
P01008	Antithrombin-III	0.006	1.560
P04004	Vitronectin	0.045	1.576
P04406	Glyceraldehyde-3-phosphate dehydrogenase	0.007	1.581
P49747	Cartilage oligomeric matrix protein	0.014	1.591
P08253	72 kDa type IV collagenase	0.008	1.610
Q99784	Noelin	0.005	1.627
Q13790	Apolipoprotein F	0.045	1.663
Q16853	Membrane primary amine oxidase	0.001	1.670
H7BYX6	Neural cell adhesion molecule 1	0.009	1.687
P02656	Apolipoprotein C-III	0.007	1.795
P33151	Cadherin-5	0.002	1.810
Q6YHK3	CD109 antigen	0.007	1.811
Q9H4G4	Golgi-associated plant pathogenesis-related protein 1	0.015	2.039
P55290	Cadherin-13	0.0004	2.079
Q08380	Galectin-3-binding protein	0.007	2.088
P23471	Receptor-type tyrosine-protein phosphatase zeta	0.012	2.230
P12830	Cadherin-1	0.028	2.255
P06727	Apolipoprotein A-IV	0.019	2.450
Q14520	Hyaluronan-binding protein 2	0.039	2.648
P05067	Amyloid-beta precursor protein	0.008	4.871

**Table S3** Identification of 192 differentially expressed proteins in serum between KFS patients and CS patients

Protein accessions	Protein descriptions	t-test P value	Ratio (KFS/CS)
Q15942	Zyxin	0.000	0.165
P0DJ19	Serum amyloid A-2 protein	0.011	0.168
P0DJ18	Serum amyloid A-1 protein	0.006	0.168
P02741	C-reactive protein	0.024	0.209
Q9Y279	V-set and immunoglobulin domain-containing protein 4	0.012	0.215
P04040	Catalase	0.000	0.217
P07738	Bisphosphoglycerate mutase	0.002	0.217
P68871	Hemoglobin subunit beta	0.022	0.232
Q02818	Nucleobindin-1	0.000	0.237
Q06830	Peroxioredoxin-1	0.001	0.244
P13647	Keratin, type II cytoskeletal 5	0.006	0.260
P01009	Alpha-1-antitrypsin	0.001	0.265
Q13228	Methanethiol oxidase	0.017	0.268
P05089	Arginase-1	0.007	0.271
Q99497	Protein/nucleic acid deglycase DJ-1	0.002	0.273
Q86Y23	Hornerin	0.005	0.276
P60174	Triosephosphate isomerase	0.000	0.290
P69905	Hemoglobin subunit alpha	0.038	0.290
P31944	Caspase-14	0.005	0.293
P60709;P63261	Actin, cytoplasmic	0.000	0.298
P07911	Uromodulin	0.013	0.300
P35527	Keratin, type I cytoskeletal 9	0.002	0.304
P02750	Leucine-rich alpha-2-glycoprotein	0.000	0.304
P00995	Serine protease inhibitor Kazal-type1	0.007	0.305
P50552	Vasodilator-stimulated phosphoprotein	0.012	0.306
Q92954	Proteoglycan 4	0.002	0.308
Q9H299	SH3 domain-binding glutamic acid-rich-like protein 3	0.004	0.311
P63104	14-3-3 protein zeta/delta	0.001	0.316
P08571	Monocyte differentiation antigen CD14	0.002	0.321
Q00151	PDZ and LIM domain protein 1	0.014	0.322
Q99941	Cyclic AMP-dependent transcription factor ATF-6 beta	0.004	0.328
P29401	Transketolase	0.010	0.329
Q8NBJ4	Golgi membrane protein 1	0.000	0.330
P22392;Q32Q12	NME1-NME2 readthrough; Nucleoside diphosphate kinase	0.000	0.332
P62937	Peptidyl-prolyl cis-trans isomerase A	0.004	0.332
Q6E0U4	Dermokine	0.001	0.333
Q9BUN1	Protein MENT	0.011	0.339
H3BTN5	Pyruvate kinase (Fragment)	0.014	0.342
Q9ULI3	Protein HEG homolog 1	0.002	0.344
O75368	SH3 domain-binding glutamic acid-rich-like protein	0.028	0.348
P08572	Collagen alpha-2(IV) chain	0.020	0.356
P24666	Low molecular weight phosphotyrosine protein phosphatase	0.000	0.363
P32942	Intercellular adhesion molecule 3	0.001	0.365
P30086	Phosphatidylethanolamine-binding protein 1	0.006	0.372
P10586	Receptor-type tyrosine-protein phosphatase F	0.003	0.377
Q7Z3B1	Neuronal growth regulator 1	0.000	0.379
Q13332	Receptor-type tyrosine-protein phosphatase S	0.007	0.380
P16070	CD44 antigen	0.012	0.386
P32119	Peroxioredoxin-2	0.017	0.386
Q9NZT1	Calmodulin-like protein 5	0.015	0.388
P00558	Phosphoglycerate kinase 1	0.001	0.399
Q92859	Neogenin	0.000	0.404
B7ZKJ8	ITIH4 protein	0.022	0.412
P02749	Beta-2-glycoprotein 1	0.000	0.414
P28072	Proteasome subunit beta type-6	0.000	0.414
P04406	Glyceraldehyde-3-phosphate dehydrogenase	0.001	0.417
O43505	Beta-1,4-glucuronyltransferase 1	0.019	0.419
A0A2R8Y619;O60814;P06899;P23527;P33778;P57053;P58876;P62807;Q16778;Q5QNW6;Q8N257;Q93079;Q96A08;Q99877;Q99879;Q99880;U3KQK0	Histone H2B	0.002	0.419
Q9P232	Contactin-3	0.003	0.419
P02671	Fibrinogen alpha chain	0.002	0.422
P30530	Tyrosine-protein kinase receptor UFO	0.001	0.432
P08294	Extracellular superoxide dismutase	0.011	0.438
Q14118	Dystroglycan	0.009	0.442
Q6UY14	ADAMTS-like protein 4	0.041	0.443
P26038	Moesin	0.002	0.446
P37802	Transgelin-2	0.021	0.449
P20933	N(4)-(beta-N-acetylglucosaminy)-L-asparaginase	0.002	0.450
O14498	Immunoglobulin superfamily containing leucine-rich repeat protein	0.020	0.451
P00451	Coagulation factor VIII	0.000	0.452
C9Y11;E7EMS7;H7BZ95;M0R0A5	Dermokine	0.002	0.462
A0A0U1RR32;A0A0U1RRH7;A0A3B3IS11;C9J0D1;P04908;P0C0S5;P0C0S8;P16104;P20671;Q16777;Q6F113;Q71UI9;Q7L7L0;Q8IUE6;Q93077;Q96KK5;Q96QV6;Q99878;Q9BTM1	Histone H2A	0.004	0.467
P00734	Prothrombin	0.011	0.471
Q9Y5Y7	Lymphatic vessel endothelial hyaluronic acid receptor 1	0.038	0.474
Q13201	Multimerin-1	0.000	0.477
P11047	Laminin subunit gamma-1	0.041	0.479
P78324;Q5TFQ8	Tyrosine-protein phosphatase non-receptor type substrate 1;Signal-regulatory protein beta-1 isoform 3	0.003	0.484
Q16270	Insulin-like growth factor-binding protein 7	0.006	0.486
P24821	Tenascin	0.018	0.490
P00568;Q5T9B7	Adenylate kinase isoenzyme 1	0.035	0.491
K7ER74	APOC4-APOC2 readthrough (NMD candidate)	0.001	0.496
P15151	Poliovirus receptor	0.000	0.498
P54108	Cysteine-rich secretory protein 3	0.000	0.504
Q9UNN8	Endothelial protein C receptor	0.014	0.505
P12830	Cadherin-1	0.010	0.507
P05155	Plasma protease C1 inhibitor	0.016	0.519
P08493	Matrix Gla protein	0.001	0.523
Q9UHG3	Prenylcysteine oxidase 1	0.009	0.525
P18206	Vinculin	0.013	0.525
P07357	Complement component C8 alpha chain	0.040	0.526
Q14847	LIM and SH3 domain protein 1	0.019	0.526
P98160	Basement membrane-specific heparan sulfate proteoglycan core protein	0.033	0.528
Q577F0	Neuropilin	0.046	0.538
P07711	Cathepsin L1	0.004	0.540
A0A087X0M8	Neural cell adhesion molecule L1-like protein	0.007	0.545
P12109	Collagen alpha-1(VI) chain	0.033	0.551
P99999	Cytochrome c	0.013	0.554
Q94919	Endonuclease domain-containing 1 protein	0.005	0.555
P02786	Transferrin receptor	0.050	0.570
P13987	CD59 glycoprotein	0.014	0.587
P48637	Glutathione synthetase	0.009	0.591
P11684	Uteroglobin	0.008	0.592
P11142	Heat shock cognate 71 kDa protein	0.001	0.604
P02652	Apolipoprotein A-II	0.028	0.605
Q6UWP8	Suprabasin	0.008	0.605
Q92520	Protein FAM3C	0.003	0.618
P15924	Desmoplakin	0.011	0.622
P12111	Collagen alpha-3(VI) chain	0.028	0.625
Q6UX71	Plexin domain-containing protein 2	0.003	0.632
P27918	Properdin	0.020	0.644
P02774	Vitamin D-binding protein	0.002	0.647
O75144	ICOS ligand	0.012	0.648
A0A0J9YYC8;A6XMV8;A6XMV9;E7EQ64;H0Y8D1;P07477;P07478;Q8NHM4	Trypsin;Protease serine 2 preproprotein	0.001	0.653
P02649	Apolipoprotein E	0.012	0.671
Q96N29	ZNF511-PRAP1 readthrough; Proline-rich acidic protein 1	0.010	0.680
P02753	Retinol-binding protein	0.047	0.684
P05556	Integrin beta-1	0.012	0.686
P33151	Cadherin-5	0.013	0.690
P02533	Keratin, type I cytoskeletal 14	0.044	0.691
Q9UGM5	Fetuin-B	0.010	1.460
Q9NPH3	Interleukin-1 receptor accessory protein	0.009	1.488
P01599	Immunoglobulin kappa variable 1-17	0.037	1.536
Q13740	CD166 antigen	0.030	1.552
Q16853	Membrane primary amine oxidase	0.006	1.583
P01718	Immunoglobulin lambda variable 3-27	0.047	1.629
Q9Y6R7	IgGfC-binding protein	0.019	1.632
P06276	Cholinesterase	0.010	1.661
P01700	Immunoglobulin lambda variable 1-47	0.001	1.706
P06310	Immunoglobulin kappa variable 2-30	0.038	1.711
Q76LX8	A disintegrin and metalloproteinase with thrombospondin motifs 13	0.035	1.733
P23470	Receptor-type tyrosine-protein phosphatase gamma	0.025	1.744
Q6YHK3	CD109 antigen	0.028	1.748
Q9BTY2	Plasma alpha-L-fucosidase	0.030	1.777
P00736	Complement C1r subcomponent	0.021	1.800
P07996	Thrombospondin-1	0.025	1.830
P07942	Laminin subunit beta-1	0.014	1.834
P43652	Afamin	0.025	1.853
A0A0B4J1V0	Immunoglobulin heavy variable 3-15	0.032	1.874
P39060	Collagen alpha-1(XVIII) chain	0.042	1.875
O75882	Attractin	0.011	1.892
P02765	Alpha-2-HS-glycoprotein	0.010	1.895
Q12913	Receptor-type tyrosine-protein phosphatase eta	0.014	1.897
P0DOY2;P0DOY3	Immunoglobulin lambda constant	0.002	1.910
P80748	Immunoglobulin lambda variable 3-9;Immunoglobulin lambda variable 3-21	0.032	1.911
A0A075B6J9	Immunoglobulin lambda variable 2-18	0.038	1.926
Q99784	Noelin	0.001	2.052
A0A075B6H9	Immunoglobulin lambda variable 4-69	0.024	2.056
P07358	Complement component C8 beta chain	0.048	2.071
P27169	Serum paraoxonase/arylesterase 1	0.004	2.074
P17813	Endoglin	0.006	2.146
P02787	Serotransferrin	0.041	2.156
P12821	Angiotensin-converting enzyme	0.012	2.168
P20023	Complement receptor type 2	0.012	2.179
P40189	Interleukin-6 receptor subunit beta	0.002	2.181
Q96IY4	Carboxypeptidase B2	0.015	2.186
A0A2Q2T2Z9	Immunoglobulin kappa variable 1-33	0.000	2.264
P03952	Plasma kallikrein	0.002	2.347
P04003	C4b-binding protein alpha chain	0.002	2.355
A0A0B4J2B5	Immunoglobulin heavy variable 3/OR16-9	0.009	2.371
P35858	Insulin-like growth factor-binding protein complex acid labile subunit	0.010	2.404
P06312	Immunoglobulin kappa variable 4-1	0.020	2.459
A2NJV5	Immunoglobulin kappa variable 2D-29	0.003	2.460
B9A064	Immunoglobulin lambda-like polypeptide 5	0.000	2.469
Q15166	Serum paraoxonase/lactonase 3	0.001	2.493
Q8IWW2	Contactin-4	0.004	2.501
A0A075B6I0	Immunoglobulin lambda variable 8-61	0.016	2.594
P05546	Heparin cofactor 2	0.030	2.625
P01860	Immunoglobulin heavy constant gamma 3	0.000	2.657
P01602	Immunoglobulin kappa variable 1-5	0.003	2.665
P01703	Immunoglobulin lambda variable 1-40	0.001	2.676
Q03591	Complement factor H-related protein 1	0.007	2.702
Q08380	Galectin-3-binding protein	0.007	2.771
P01701	Immunoglobulin lambda variable 1-51	0.002	2.790
A0A075B6I9	Immunoglobulin lambda variable 7-46	0.010	2.817
P02745	Complement C1q subcomponent subunit A	0.000	3.028
P29622	Kallistatin	0.002	3.031
P01857	Immunoglobulin heavy constant gamma 1	0.000	3.067
P22792	Carboxypeptidase N subunit 1	0.001	3.121
Q9Y4L1	Hypoxia up-regulated protein 2	0.048	3.124
P15814	Immunoglobulin lambda-like polypeptide 1	0.003	3.159
P02768	Serum albumin	0.004	3.222
P01859	Immunoglobulin heavy constant gamma 2	0.013	3.228
P01768;P0DP03	Immunoglobulin heavy variable 3-30	0.002	3.289
P05090	Apolipoprotein D	0.006	3.589
P06681	Complement C2	0.001	3.689
P01780	Immunoglobulin heavy variable 3-7	0.000	3.708
P01834	Immunoglobulin kappa constant	0.000	3.734
O75636	Ficolin-3	0.002	4.294
P08603	Complement factor H	0.001	4.380
P01871	Immunoglobulin heavy constant mu	0.010	4.454
P13598	Intercellular adhesion molecule 2	0.004	4.476
A0A0C4DH34	Immunoglobulin heavy variable 4-28	0.000	4.481
P01824;P01825;P06331;P0DP06;P0DP08	Immunoglobulin heavy variable 4-39;Immunoglobulin heavy variable 4-59;Immunoglobulin heavy variable 4-34;Immunoglobulin heavy variable 4-30-4;Immunoglobulin heavy variable 4-38-2	0.018	7.442